*2011 International Nuclear Atlantic Conference - INAC 2011*
*Belo Horizonte,MG, Brazil, October 24-28, 2011*
*ASSOCIAÇÃO BRASILEIRA DE ENERGIA NUCLEAR - ABEN*
***ISBN:*** **978-85-99141-04-5**

# CHARACTERIZATION OF HDR Ir-192 SOURCE FOR 3D PLANNING SYSTEM

**Gabriel P. Fonseca.[1], Hélio Yoriyaz[1], Paula C. G. Antunes[1], Paulo T. D. Siqueira[1], Rodrigo Rubo[2], Renato A. Minamisawa[3], Louise A. Ferreira[4]**

[1] Instituto de Pesquisas Energéticas e Nucleares (IPEN / CNEN - SP)
Av. Professor Lineu Prestes, 2242
05508-000 São Paulo, SP
gabriel.fonseca@usp.br
hyoriyaz@ipen.br
pacriguian@gmail.com
ptsiquei@ipen.br

[2]Hospital das Clínicas da Faculdade de Medicina da Universidade de São Paulo (HC/FMUSP)
Serviço de Radioterapia
Av. Dr. Enéas de Carvalho Aguiar, 255 – 3º andar
05403-001 São Paulo, SP
rarubo@yahoo.com.br

[3]Paul Scherrer Institut (PSI)
5232 Villigen PSI, Switzerland
renato.minamisawa@psi.ch

[4]Universidade Estadual de Maringá (UEM)
Faculdade de Medicina
Av. Colombo, 5.790
87020-900 Maringá, PR
louiseferreira@gmail.com

## ABSTRACT

Brachytherapy treatment involves surgical or cavitary insertion of radiotactive sources for diseases treatments, such as: lung, gynecologic or prostate cancer. This technique has great ability to administer high doses to the tumor, with adjacent normal tissue preservation equal or better than external beam radiation therapy. Several innovations have been incorporated in this treatment technique, such as, 3D treatment planning system and computer guided sources. In detriment to scientific advances there are no protocols that relate dose with tumor volume, organs or A point, established by ICRU38 and used to prescribe dose in treatment planning system. Several international studies, like as EMBRACE, the multicentre international study, has been trying to correlate the dose volume using 3D planning systems and medical images, as those obtained by CT or MRI, to establish treatment protocols. With the objective of analyzing the 3D dose distribution, a microSelectron-HDR remote afterloading device for high dose-rate (HDR) was characterized in the present work. Through the data provided by the manufacturer the source was simulated, using the MCNP5 code to calculate American Association of Physicists in Medicine Task Group No. 43 report (AAPM TG43) specified parameters. The simulations have shown great agreement when compared to the ONCENTRA® planning system results and those provided by literature. The microSelectron-HDR remote afterloading device will be utilized to simulate 3D dose distribution through CT images processed by an auxiliary software which process DICOM images.

## 1. INTRODUCTION

Brachytherapy treatment involves surgical or cavitary insertion of radioactive source for disease treatments, such as: lung, gynecologic or prostate cancer. This technique has great ability to administer high doses into the tumor, with adjacent normal tissue preservation equal or better than external beam radiation therapy [1]. Furthermore, this technique is cheaper than high technology external beam radiation, factor of particular interest to developing countries.

Recently, several innovations have been incorporated in this treatment technique worldwide, such as, 3D treatment planning system and computer guided sources. However, in detriment to scientific advances there are no protocols that relate dose with tumor volume, organs or A point, established by ICRU38 [2] and used to prescribe dose in treatment planning system. This point dismisses the tumor volume and in the practice depends only of the applicator position, which can be inside or outside of a tumor resulting in over or underdosing [3;4;5]. International studies, as EMBRACE [6;7], a multicentre international study, has been trying to correlate dose-volume using 3D planning systems and medical images, as CT or MRI, to establish treatment protocols.

To analyze 3D dose distribution, first of all, the source utilized at *Serviço de Radioterapia do Hospital das Clínicas* was characterized based on parameters established by the Task Group 43 (TG43) [8]. The microSelectron-HDR remote afterloading device for high dose-rate (HDR) consists of an internal Ir-192 active source, with initial activity of 12.4 Ci, enveloped by a steel capsule with a length of 4.95 mm and an outer diameter of 0.9 mm. Using the data provided by the manufacturer, the source was simulated with the MCNP5 (Monte Carlo N-Particle) code [9] to calculate air kerma strength, dose rate constant, polar dose profile, dose rate, anisotropy function and radial dose profile. The results obtained from simulation were compared with those provided by ONCENTRA® (Nucletron´s Planning System) relative dose profile and with literature. This source will be utilized to simulate 3D dose distribution through CT images processed by an auxiliary software which process DICOM images, identify structures, organ composition, densities and insert this data into the MCNP5 input file, allowing simulations of real patients and a 3D dose distribution study.

## 2. MATERIAL AND METHODS

### 2.1. MicroSelectron-HDR Radioactive Source

The $^{192}$Ir remote afterloading source (Fig. 1) for HDR brachytherapy consists of a pure iridium metal cylinder (0.65 mm in diameter and 3.60 mm long) with $^{192}$Ir uniformly distributed in the volume and encapsulated in a AISI316L steel (0.08% C, 17.1 % Cr, 65.25% Fe, 2% Mn, 2.5% Mo, 12% Ni, 0,04 P, 1 % Si, 0.03 S) with an outer diameter of 0.90 mm and 4.50 mm long. The mechanical dimensions and material compositions were provided by Nucletron, except the cable density obtained experimentally by Daskalov [10].

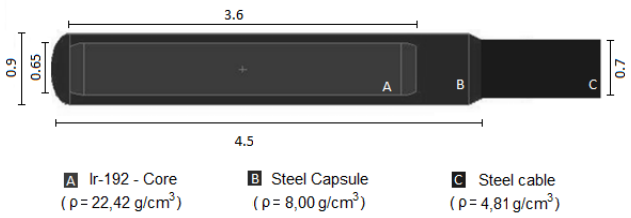


**Fig.1. MicroSelectron-HDR $^{192}$Ir illustrative source design. All dimensions are in mm.**

## 2.2 Monte Carlo Based Code

Monte Carlo method simulates the radiation transport through a stochastic process based on physical and statistical principles of radiation transport and particles interaction. The processors and code evolution has caused the appearance of many software based on Monte Carlo method to be used in patients treatment planning in hospitals or clinical studies [11;12;13].

The MCNP code, released in 1977 and continually improved, was developed by Los Alamos laboratory and emerged from works done during World War II, generally attributed to Fermi, von Neumann, Ulam, Metropolis and Richtmyer who used Monte Carlo method for solving transport problems [9]. This code simulates electrons, neutrons and photons in a wide energy range through a stochastic process based on physical and statistical principles of radiation transport and particles interaction.

In this work a microSelectron-HDR source utilized in brachytherapy was characterized using MCNP5. The simulations were performed using an Ir-192 National Nuclear Data Center (NNDC) spectrum and transporting photons without energy cut-off, using the MCPLIB04 photon cross-section library in Mode P which uses Thick Target Bremsstrahlung (TTB) model where secondary electrons were generated in the direction of the incident photon and are immediately annihilated, after generating bremsstrahlung [9].

### 2.2.1 Ir-192 energy spectrum

**Table 1. Ir-192 photon spectrum, obtained from NNDC, with photon energy (MeV) and the average intensity (%). * K-shell originated from electron capture. ** K-shell originated from $\beta^-$ decay.**

| Energy (MeV) | Intensity (%) | Energy (MeV) | Intensity (%) |
|---|---|---|---|
| 0.0615* | 0.4120 | 0.3292 | 0.0060 |
| 0.0630* | 0.7039 | 0.3745 | 0.2493 |
| 0.0651** | 1.1309 | 0.4165 | 0.2877 |
| 0.0668** | 1.9178 | 0.4205 | 0.0237 |
| 0.0711* | 0.0827 | 0.4681 | 20.5587 |
| 0.0714* | 0.1600 | 0.4846 | 1.0942 |
| 0.0734* | 0.0560 | 0.4853 | 0.0010 |
| 0.0754** | 0.2292 | 0.4891 | 0.1504 |
| 0.0757** | 0.4408 | 0.5886 | 1.9423 |
| 0.0778** | 0.1570 | 0.5935 | 0.0181 |
| 0.1104 | 0.0042 | 0.5994 | 0.0017 |
| 0.1363 | 0.0860 | 0.6044 | 3.5261 |
| 0.1770 | 0.0018 | 0.6125 | 2.2962 |
| 0.2013 | 0.1624 | 0.7039 | 0.0018 |
| 0.2058 | 1.1468 | 0.7658 | 0.0006 |
| 0.2803 | 0.0039 | 0.8845 | 0.1251 |
| 0.2833 | 0.0913 | 1.0615 | 0.0228 |
| 0.2960 | 12.3498 | 1.0899 | 0.0005 |
| 0.3085 | 12.7626 | 1.3782 | 0.0005 |
| 0.3165 | 35.5660 | | |

The Ir-192 decays by $\beta^-$ (95.6%) to excited states of Pt-192 and by electron capture to excited states of Os-192 (4.6%), with 2.363 photons average emission in one decay. The complete spectrum was obtained from NNDC (National Nuclear Data Center) [14] including β particles, photons and characteristics X-Ray (energy below 78 keV) of which only photons with energy above 78 keV are considered in most works since β particles and characteristics X-Ray are shielded by the outer capsule. However in this work the iridium and daughter nucleus K-shell X-Ray were considered since the simulation time does not differ considerably and a previous work showed differences [15], although small, in the air kerma strength result.

The simulated spectrum (table 1) presents average energy of 0.355 and 0.372 MeV with and without characteristics X-Ray, respectively. The average energy without X-ray differs in only 0.5% from TG43 declared value (0.370 MeV).

### 2.2.2 Track length estimator tally (F4)

The deposited energy was calculated through a track length estimator tally (F4) which estimates a cell average flux by summing all particle tracks in a cell as described in the following equation:

$$\bar{\phi}_v = \frac{1}{V}\sum W T_l \qquad (1)$$

$\bar{\phi}_v$ = cell average flux;
$V$ = cell volume;
$W$ = particle weight;
$T_l$ = track length.

The track length estimator tally (F4) in units of particle per $cm^2$ was converted into deposited energy using the MCNP5 cards DE (Dose Energy Card) and DF (Dose Function Card) and using a track length cell energy deposition tally (F6), as described below.

#### 2.2.2.1 Energy deposition – DE/DF cards

The F4 tally, in units of particle per $cm^2$, in a vacuum cell was converted in air-kerma (MeV/g) using LOG-LOG interpolations, as recommended [9], using DE and DF cards, where DE is the energy and DF is a mass energy transfer coefficient ($\mu_{tr}/\rho$) to dry air at sea level (0.0124% C, 75,5268% N, 23,1781% N and 1,2827% Ar) with density $1.205 \times 10^{-3}$ $g/cm^3$, obtained from National Institute of Standards and Technology (NIST) [16] (table 2). This process was performed to determine the air kerma (described at subsection 2.3.1) through simulation in vacuum which eliminates air attenuation and scattering interference.

**Table 2. Mass energy transfer coefficient to dry air, obtained from NIST, used as MCNP DE/DF cards to calculate air kerma.**

| Mass Energy Transfer Coefficient to Dry Air | |
|---|---|
| Energy (MeV) | $\mu_{tr}/\rho$ (cm$^2$/g) |
| DE | DF |
| 0.005 | 39.3100 |
| 0.006 | 22.7000 |
| 0.008 | 9.4460 |
| 0.010 | 4.7420 |
| 0.015 | 1.3340 |
| 0.020 | 0.5389 |
| 0.030 | 0.1537 |
| 0.040 | 0.0683 |
| 0.050 | 0.0410 |
| 0.060 | 0.0304 |
| 0.080 | 0.0241 |
| 0.100 | 0.0233 |
| 0.150 | 0.0250 |
| 0.200 | 0.0267 |
| 0.300 | 0.0287 |
| 0.400 | 0.0295 |
| 0.500 | 0.0297 |
| 0.600 | 0.0295 |
| 0.800 | 0.0282 |
| 1.000 | 0.0279 |
| 1.250 | 0.0267 |

### 2.2.2.2 Track length cell energy deposition tally (F6)

The track length cell energy deposition tally (F6), utilized to calculate the deposited energy only by photons, consists basically in a track length tally multiplied by a reaction rate convolved with a energy-dependent heating function, as described in the following equation:

$$H_t = WT_l\sigma_t(E)H(E)\frac{\rho_a}{m} \quad (2)$$

$\sigma_t(E)$ = microscopic total cross section (barns);
$H(E)$ = heating number (MeV/collision);
$\rho_a$ = atom density (atoms/barn-cm);
$m$ = cell mass (g);
$T_l$ = track lenght (cm).

### 2.3 Simulations of Source Parameters

The source parameters like air kerma, air kerma strength, dose rate constant, anisotropy function, geometric factor and radial dose profile were defined by TG43 [8], allowing analytical dose calculation, based on experimental and/or simulated parameters.

#### 2.3.1 Air kerma strength

Air kerma strength ($S_k$), in units of U (1 U = 1 cGycm$^2$h$^{-1}$), represents the brachytherapy source strength and is specified in terms of air kerma rate ($\dot{K}_{air}(d)$) at the point with distance along the transverse axis of the source in free space. This distance, d, can be any large distance enough that the source may be treated as a point, usually defined at 1 m.

$$S_k = \dot{K}_{air}(d).d^2 \tag{3}$$

The air kerma strength per unit contained activity ($S_k/A$) in units of μGym$^2$h$^{-1}$Bq$^{-1}$, was calculated using air-kerma simulated at $r = 1$ m and $\theta = \pi/2$ in a cylindrical vacuum cell with 10 cm diameter and 2 mm long, in a vacuum sphere, using the process described by Borg [15]. The result obtained with MCNP5 track length estimator tally (F4) was converted to air-kerma per particle ($K'_{air}(d)$), in units of MeV.g$^{-1}$.particle$^{-1}$, using the MCNP5 DE/DF cards, as described in section 2.2.2.1, and converted in air kerma rate with the following equation:

$$\dot{K}_{air}(d) = 2.363\,.\,1{,}602.10^{-10}\,.K'_{air}(d).A \tag{4}$$

Where:

2,363 = average number of photons in one decay;
1,602.10$^{-10}$ = convertion factor from MeV/g to Gy;

Using equations 3 and 4 the air kerma strength per unit contained activity can be defined as:

$$S_k/_A = 3{,}786.10^{-10}.\,K'_{air}(d).d^2\ [Gym^2s^{-1}Bq^{-1}] \tag{5}$$

or

$$S_k/_A = 1{,}363\,.K'_{air}(d).d^2\ [UBq^{-1}] \tag{6}$$

#### 2.3.2 Dose rate constant ($\wedge$)

The dose rate constant ($\wedge$) is defined as the dose rate to water at a distance of 1 cm on the transverse axis of air kerma strength unit in a water phantom:

$$\wedge = \dot{D}(r_{0,\theta})/S_k \tag{7}$$

The dose at $r = 1$ cm and $\theta = \pi/2$ ($D(r_{0,\theta})$) in a water sphere (radii 0.05 cm) was simulated in a 40x40x40 $cm^3$ water phantom using the MCNP5 F6 tally.

### 2.3.3 Anisotropy function

Anisotropy function ($F(r,\theta)$) accounts for the anisotropy of dose distribution around the source, including the effects of absorption and scatter in the medium. It was simulated around the source in radii (r) of 0.25, 0.5, 1, 2, 3 and 5 cm, the dose was calculated in water spheres (radii: 0.0625 mm for r = 0.25 cm; 0.125 mm for r = 0.5 cm; 0.25 mm for r=1 cm; 0.5 mm for r = 2, 3 e 5 cm) inside a 40x40x40 $cm^3$ water phantom using the F6 tally. Fig. 2 represents the parameters utilized without the presence of the source cable which was considered in the simulations.

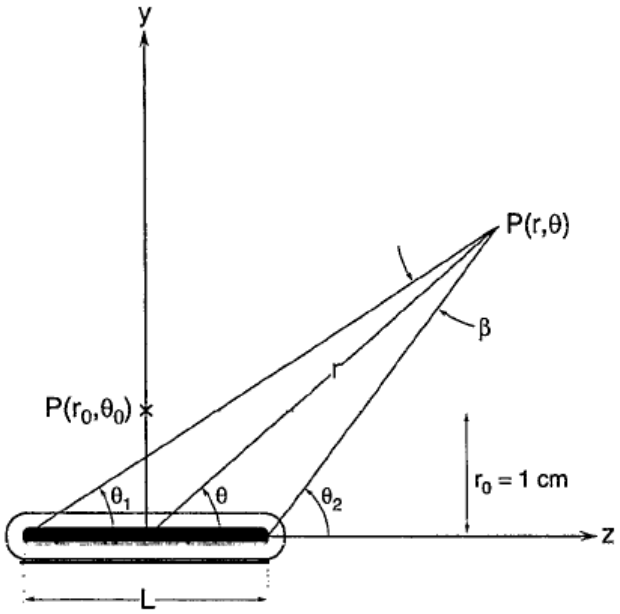


**Fig. 2. Representation of the geometry considered in the TG43 formalism [8]**

The anisotropy function is defined by:

$$F(r,\theta) = \frac{\dot{D}(r,\theta)}{\dot{D}(r,\theta_0)} \frac{G_L(r,\theta_0)}{G_L(r,\theta)} \quad (8)$$

Where:

$\theta_0 = {}^{\pi}/_{2}$;
$\dot{D}(r,\theta)$ = dose in the point $(r,\theta)$;
$\dot{D}(r,\theta_0)$ = dose in the point $(r,\theta_0)$;
$G_L(r,\theta)$ = geometric factor in the point $(r,\theta)$;

$G_L(r,\theta_0)$ = geometric factor in the point $(r,\theta_0)$.

The geometric factor accounts for the variation of relative dose due only to the spatial of activity. For a linear source the geometric factor is defined as [17]:

$$G_L \quad (r,\theta) = \begin{cases} \dfrac{\beta}{Lr\sin\theta} \;\; if\ \theta \neq 0 \\ (r^2 - {L^2}/{4})^{-1} \;\; if\ \theta = 0 \end{cases} \tag{9}$$

Where:

$\beta = \theta_2 - \theta_1$ (Fig. 2)

### 2.3.4 Radial dose function

Radial dose function applies only to the transversal axis and considers the absorption and scatter over this axis. This was simulated from 0.1 to 9 cm from the center of the source and characterized in water spheres (radii 0.025 cm) inside a water phantom similar as utilized to obtain the polar dose profile.

$$g(r) = \frac{\dot{D}(r,\theta_0).G(r_0,\theta_0)}{\dot{D}(r_0,\theta_0).G(r,\theta_0)} \tag{10}$$

### 2.3.6 ONCENTRA® planning system

Oncentra® (4.0) is a software for both external beam and brachytherapy treatment planning used for 3D-planning based on CT or MRI and semi-orthogonal reconstruction. This software calculates the dose based on AAPM Task Group 43 dose-calculation formalism and was used to calculate the dose profile parallel to longitudinal catheter axis, at distance 0.5 cm, for two dwell positions, 0 and 10 cm, with dwell time of 1s. This profile was calculated in a water phantom and characterized in a 10 cm long route in steps of 0.5 cm and used to compare with MCNP5 simulated profile.

## 3 RESULTS AND DISCUSSIONS

### 3.1 Air Kerma Strength

The air kerma at 1 m distant from the source is $(7.19 \pm 0.04)\text{x}10^{-8}$ MeV.g$^{-1}$.particle$^{-1}$. Using equation 6 the air kerma strength per contained activity unit is $(9.79 \pm 0.06\text{x}10^{-8}$ UBq$^{-1}$. This value differ in 0.7 % comparing to the result obtained by Borg [15], $9.72\text{x}10^{-8}$ UBq$^{-1}$. This difference is approximately the uncertainty value and may be due to small differences in simulated spectrum and/or geometry of the source.

### 3.2 Dose Rate Constant ($\Lambda$)

The dose in water at point $(r_{0,\theta})$ is (1.086 ± 0.008).A.$10^{-7}$ cGyh$^{-1}$, where A is the source activity, using this value in equation 7, with air kerma strength of (9.79 ± 0.06).A.$10^{-8}$ U, the dose rate constant is $\Lambda =$ (1.109 ± 0.011) cGyh$^{-1}$U$^{-1}$. This result is in good agreement with values, 1.108 cGyh$^{-1}$U$^{-1}$, 1.109 cGyh$^{-1}$U$^{-1}$ and 1.12 cGyh$^{-1}$U$^{-1}$, presented by Daskalov [10], Taylor [18] and TG43[8], respectively.

### 3.3 Anisotropy Function

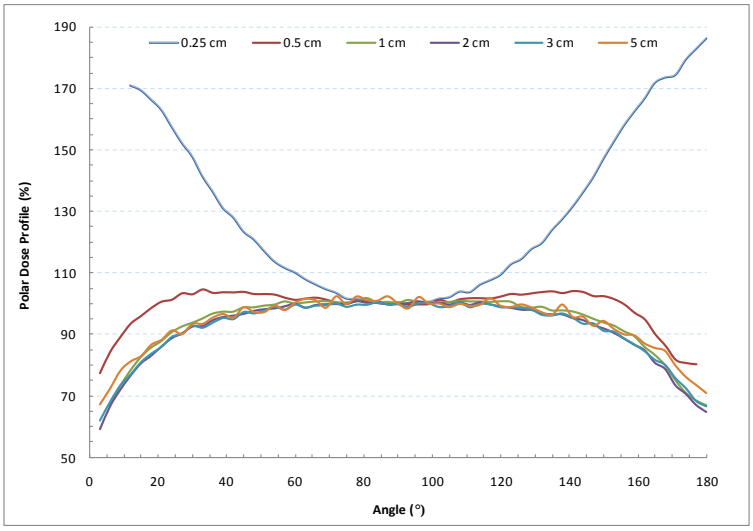


**Fig. 3 Polar dose profiles normalized to dose at θ = $\pi/2$ in a water phantom at various source distances.**

The polar dose profile for microSelectron-HDR source (Fig. 3) was normalized for each distance at the transverse axis (θ = $\pi/2$). The results obtained show uncertainty lower than 1 %. For r = 0.25 cm the maximum dose occurs at angles θ = 12° (smaller angles weren´t simulated since their position coincide with the cable position) and 180°, this effect occur because this radii is near a half source length, so these points are very close of the source.

The table 3 presents the anisotropy function derived from polar dose profile for radii between 0.25 and 5 cm. The results show lower sensitivity values of $F(r,\theta)$ for small radii due to the geometric factor. The results have shown good agreement with those obtained from Daskalov [10]. The difference is lower than 1 % for most points especially for radii between 0.5 an 3 cm, with some points with maximum difference of 5 % and 3 %, for radii 0.25 and 5 cm, respectively.

**Table 3. Anisotropy function $F(r,\theta)$ derived from polar dose profile for microSelectron-HDR $^{192}$Ir (polar angle specified relative to the source cable).**

| Polar Angle Degrees | Distance from activity source center (cm) | | | | | |
|---|---|---|---|---|---|---|
| | 0.25 | 0.5 | 1 | 2 | 3 | 5 |
| 3 | - | - | - | 0.587 | 0.616 | 0.669 |
| 6 | - | 0.647 | 0.635 | 0.661 | 0.678 | 0.722 |
| 9 | - | 0.707 | 0.698 | 0.715 | 0.731 | 0.779 |
| 12 | 0.797 | 0.751 | 0.748 | 0.760 | 0.767 | 0.810 |
| 15 | 0.831 | 0.792 | 0.791 | 0.799 | 0.806 | 0.827 |
| 21 | 0.890 | 0.846 | 0.844 | 0.854 | 0.857 | 0.880 |
| 27 | 0.922 | 0.883 | 0.892 | 0.897 | 0.899 | 0.899 |
| 30 | 0.941 | 0.910 | 0.906 | 0.919 | 0.926 | 0.932 |
| 39 | 0.951 | 0.937 | 0.947 | 0.952 | 0.952 | 0.964 |
| 42 | 0.966 | 0.948 | 0.949 | 0.957 | 0.948 | 0.953 |
| 51 | 0.977 | 0.968 | 0.975 | 0.979 | 0.977 | 0.971 |
| 57 | 0.981 | 0.982 | 0.993 | 0.990 | 0.981 | 0.978 |
| 60 | 0.991 | 0.980 | 0.988 | 0.998 | 0.997 | 1.002 |
| 63 | 0.992 | 0.980 | 0.993 | 0.986 | 0.987 | 1.014 |
| 75 | 0.991 | 0.992 | 0.999 | 1.000 | 0.991 | 0.997 |
| 87 | 0.998 | 1.000 | 1.004 | 0.998 | 0.999 | 1.023 |
| 90 | 1.000 | 1.000 | 1.000 | 1.000 | 1.000 | 1.000 |
| 93 | 0.998 | 1.002 | 1.010 | 1.003 | 0.991 | 0.983 |
| 105 | 0.995 | 1.001 | 1.001 | 0.997 | 0.993 | 0.988 |
| 120 | 0.984 | 0.978 | 0.995 | 0.990 | 0.988 | 0.991 |
| 129 | 0.981 | 0.966 | 0.969 | 0.976 | 0.980 | 0.986 |
| 135 | 0.969 | 0.957 | 0.956 | 0.961 | 0.960 | 0.962 |
| 141 | 0.955 | 0.936 | 0.948 | 0.948 | 0.953 | 0.954 |
| 147 | 0.940 | 0.922 | 0.921 | 0.925 | 0.934 | 0.926 |
| 150 | 0.935 | 0.902 | 0.907 | 0.913 | 0.909 | 0.941 |
| 156 | 0.908 | 0.878 | 0.876 | 0.879 | 0.884 | 0.897 |
| 162 | 0.862 | 0.827 | 0.825 | 0.842 | 0.842 | 0.868 |
| 165 | 0.843 | 0.803 | 0.798 | 0.801 | 0.814 | 0.853 |
| 168 | 0.810 | 0.758 | 0.765 | 0.780 | 0.797 | 0.843 |
| 171 | 0.778 | 0.723 | 0.718 | 0.728 | 0.754 | 0.796 |
| 174 | 0.772 | 0.683 | 0.678 | 0.700 | 0.722 | 0.759 |
| 177 | 0.769 | 0.673 | 0.654 | 0.665 | 0.680 | 0.733 |

**Table 4. Radial dose function obtained with MCNP5, compared with the results obtained by Daskalov[9] and the presented by TG43[8].**

| Distance (cm) | Radial Dose Function | | |
|---|---|---|---|
| | MCNP5 | Daskalov | TG43 |
| 0.10 | 1.004 | 1.004 | - |
| 0.20 | 1.001 | 1.000 | - |
| 0.30 | 1.000 | 1.001 | - |
| 0.40 | 1.000 | 0.987 | - |
| 0.50 | 1.001 | 1.000 | 0.994 |
| 1.00 | 1.000 | 1.000 | 1.000 |
| 1.50 | 1.002 | 1.003 | 1.010 |
| 2.00 | 1.002 | 1.007 | 1.010 |
| 2.50 | 1.013 | 1.008 | 1.010 |
| 3.00 | 1.009 | 1.008 | 1.020 |
| 4.00 | 1.003 | 1.004 | 1.010 |
| 5.00 | 0.995 | 0.995 | 0.996 |
| 6.00 | 0.974 | 0.981 | 0.972 |
| 7.00 | 0.961 | 0.964 | 0.942 |
| 8.00 | 0.947 | 0.940 | 0.913 |
| 9.00 | 0.926 | 0.913 | 0.891 |

### 3.4 Radial Dose

The radial dose function ($g(r)$) with uncertainty of 1%, was calculated using equation 10. The results obtained were compared (table 4) with the results obtained by Daskalov [9] and presented by TG43[8].

The maximum difference between the results obtained in this work is 1.36% and 3.74%, comparing to values provided by Daskalov and TG43, respectively. However, the results showed by TG43 were not obtained with exactly the same source, with slightly geometric design differences and probably different capsule composition.

### 3.5 Relative Dose Profile

The relative dose profile obtained with MCNP5 and Oncentra® (Fig. 4), was normalized at position 0 cm and shows good agreement with differences lower than 0.3 % in points with relative dose greater than 9 % and maximum difference of 3.9 % at point with relative dose of 2%.

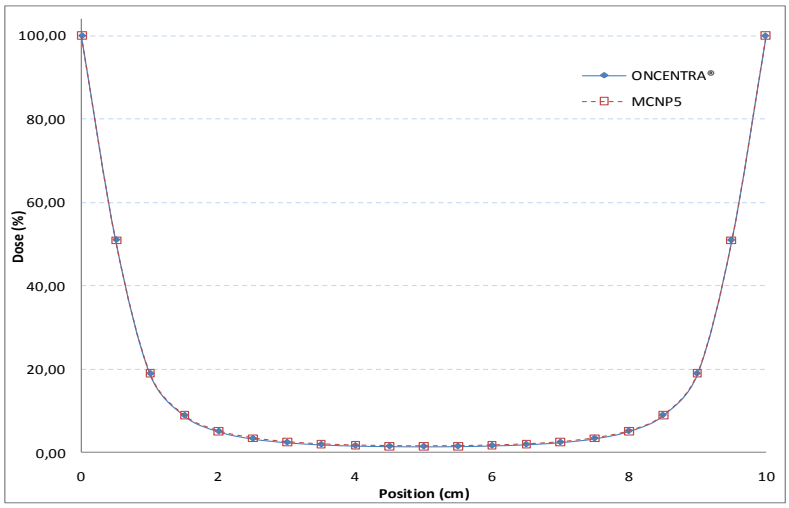


**Fig. 4. Relative dose profile obtained with MCNP5 compared to the Oncentra® profile at 5 mm distance from the source for two dwell positions, 0 and 10 cm, with dwell time 1 s.**

## 4. CONCLUSIONS

The real patients simulations will be performed identifying the organs geometry and composition, obtained through the gray scale and the Hounsfield number. Since the Ir-192 present photons with short range and high dose gradient the results accuracy depends on the body and the source geometry representation in the voxel phantom. To verify the representation of source the simulations results were compared with bibliographic data.

The results obtained from MCNP5 simulations including all the parameters specified by TG43 to characterize the source and the dose distribution, allowing analytical dose calculate, show a great agreement with the bibliographic data and Oncentra® planning system, validating the simulations since the most of the results presented differences near or lower than uncertainty. Although the results present a great agreement, in a future work this

simulations will be validated experimentally through measures with TLD, MOSFET, radiographic films and OSL dosimeters in a tissue equivalent phantoms allowing simulations of real patients in a voxel phanton through CT or MRI images with great accuracy.

## ACKNOWLEDGMENTS

We would like to express our gratitude to "*Serviço de Radioterapia do Hospital das Clínicas da Universidade de São Paulo*" team for their experimental and theoretical support.

## REFERENCES

1. Georg D, Kirisits C, Hillbrand M, Dimopoulos J, Pötter R, "Image-guided brachytherapy for cervix cancer: high-tech external beam therapy versus high-tech brachytherapy". *Int J Radiat Oncol Biol Phys*. **Vol. 4**, pp. 1272-8 (2008).
2. International Commission on Radiation Units and Measurements (ICRU) "Report 38: Dose and volume specification for reporting intracavitary therapy in gynecology". *Bethesda: International Commission on Radiological Units and Measurements* (1985).
3. Pierquin B, Wilson J.F, Chassagne D, et al, "Modern brachytherapy" *New York: Masson* (1987).
4. Khan F, "The physics of radiation therapy" *Lippincott Williams and Wilkins.* Baltimore (1994).
5. Lanciano R, "Optimizing radiation parameters for cervical cancer", *Radiation Oncology*, **Vol. 10**, pp. 36-43, 2006
6. Haie-Meder C, Potter R, Van Limbergen E, Briot E, De Brabandere M, Dimopoulos J, Dumas I, Hellebust TP, Kirisits C, Lang S, Muschitz S, Nevinson J, Nulens A, Petrow P, Wachter-Gerstner N; "Gynaecological (GYN) GEC-ESTRO Working Group. Recommendations from Gynaecological (GYN) GEC-ESTRO Working Group (I): concepts and terms in 3D image based 3D treatment planning in cervix cancer brachytherapy with emphasis on MRI assessment of GTV and CTV". *Radiotherapy and Oncology*. **Vol 74**, pp. 235-45 (2005).
7. Potter R, Haie-Meder C, Van Limbergen E, Barillot I, De Brabandere M, Dimopoulos J, Dumas I, Erickson B, Lang S, Nulens A, Petrow P, Rownd J, Kirisits C; "GEC ESTRO Working GroupRecommendations from gynaecological (GYN) GEC ESTRO working group (II): concepts and terms in 3D image-based treatment planning in cervix cancer brachytherapy-3D dose volume parameters and aspects of 3D image-based anatomy, radiation physics, radiobiology". *Radiotherapy and Oncology*. **Vol. 78**, pp. 67-77 (2006).
8. Ravinder N, et al. AAPM Technical Report 51: "Dosimetry of Interstitial Brachytherapy Sources". American Association of Physicists in Medicine Task Group 43. *Med. Phys*. **Vol 22**, (1995).
9. Briesmeister, J.F. "MCNP: A general Monte Carlo N-particle transport code, version 5". *Los Alamos Scientific Laboratory*, Los Alamos, New México (2008).
10. Daskalov, G.M, et al. "Monte Carlo-aided dosimetry of a new high dose-rate brachytherapy source" *Med. Phys*. **Vol 25**, pp. 2200-8 (1998).
11. Stabin, M.G. "Monte Carlo modeling of radiation dose distributions in intravascular radiation therapy". *Med. Phys*. **Vol**. **27**, pp. 1086-92 (2000).
12. Yoriyaz H. "Absorbed fractions in a voxel-based phantom calculated with the MCNP-4B code". *Med. Phys.*, **Vol. 27**, pp .l555-62 (2000).
13. Evans J.E. "Absorbed dose estimates to structures of the brain and head using a high-resolution voxel-based head phantom". *Med. Phys*., **Vol. 28**, pp.78O-86 (2001).

14. Coral M. Baglin "NuDat 2.5" *National Nuclear Data Center*, http://www.nndc.bnl.gov/nudat2/reCenter.jsp?z=77&n=115 (1998).
15. Borg, J, Rogers D.W.O. "Monte Carlo Calculations of Photon Spectra in Air from $^{192}$Ir Sources". *Institute for National Measurement Standards*, Ottawa, Canadá (1999).
16. "X-Ray mass attenuation Coefficients" National Institute of Standards and Technology (NIST), http://physics.nist.gov/PhysRefData/XrayMassCoef/ComTab/air.html (2011).
17. Rivard et al. Technical Report 84 - Update of AAPM Task Group No. 43 Report: "A revised AAPM protocol for brachytherapy dose calculations". American Association of Physicists in Medicine Task Group 43. *Med. Phys*. **Vol 31**, (2004).
18. R E. P. Taylor, D. W. O. Rogers, "EGSnrc Monte Carlo calculated dosimetry parameters for 192Ir and 169Yb brachytherapy sources". *Med. Phys.* **Vol. 35**, pp. 4933-44 (2008).